Journal of Materials Science: Materials in Medicine _####################_
https://doi.org/10.1007/s10856-020-06374-w

TISSUE ENGINEERING CONSTRUCTS AND CELL SUBSTRATES

Original Research

Bioprinting predifferentiated adipose-derived mesenchymal stem cell spheroids with methacrylated gelatin ink for adipose tissue engineering

Julien Colle[1,2] · Phillip Blondeel[2] · Axelle De Bruyne[1] · Silke Bochar[1] · Liesbeth Tytgat[3] · Chris Vercruysse[1] · Sandra Van Vlierberghe[3] · Peter Dubruel[3] · Heidi Declercq[1]

Received: 7 September 2019 / Accepted: 3 March 2020

Abstract

The increasing number of mastectomies results in a greater demand for breast reconstruction characterized by simplicity and a low complication profile. Reconstructive surgeons are investigating tissue engineering (TE) strategies to overcome the current surgical drawbacks. 3D bioprinting is the rising technique for the fabrication of large tissue constructs which provides a potential solution for unmet clinical needs in breast reconstruction building on decades of experience in autologous fat grafting, adipose-derived mesenchymal stem cell (ASC) biology and TE. A scaffold was bioprinted using encapsulated ASC spheroids in methacrylated gelatin ink (GelMA). Uniform ASC spheroids with an ideal geometry and diameter for bioprinting were formed, using a high-throughput non-adhesive agarose microwell system. ASC spheroids in adipogenic differentiation medium (ADM) were evaluated through live/dead staining, histology (HE, Oil Red O), TEM and RT-qPCR. Viable spheroids were obtained for up to 14 days post-printing and showed multilocular microvacuoles and successful differentiation toward mature adipocytes shown by gene expression analysis. Moreover, spheroids were able to assemble at random in GelMA, creating a macrotissue. Combining the advantage of microtissues to self-assemble and the controlled organization by bioprinting technologies, these ASC spheroids can be useful as building blocks for the engineering of soft tissue implants.

1 Introduction

Breast cancer is the most common cancer in women worldwide, with nearly 1.7 million new cases diagnosed in 2012 (second most common cancer overall). This represents about 12% of all new cancer cases and 25% of all cancers in women [1]. Mastectomies impair the esthetic appearance, function and psychological well-being of patients. In addition to breast reconstruction following mastectomy for established breast cancer, an increasing number of women with BRCA mutations (25%) is opting for prophylactic mastectomy followed by breast reconstruction, indicating the need for soft tissue implants [2]. The success of conventional implant-based breast reconstruction has been hindered by complications such as capsular contracture, infection, rupture, foreign body reaction and anaplastic large-cell lymphoma [3]. Adipose tissue (AT), in the form of a free flap, has been the preferred method of choice since patients are pleased with the natural shape, consistency and permanency of the superior esthetic results [4]. Despite major advancements in microsurgery and transplantation, reconstruction remains hindered by the availability of donor sites. Even in less extensive cases, the harvest of donor tissue carries a significant risk of donor site morbidity and the potential for failure, infection, and degradation at the host site. The microvascular nature of the surgical procedure makes it a costly solution and requires a high level of surgical skill [5]. Surgeons are persistently attempting to optimize surgical techniques and investigating new

✉ Julien Colle
julien.colle@ugent.be

[1] Tissue Engineering Group, Bioprint Facility-Department of Human Structure and Repair-Faculty of Medicine and Health Sciences, Ghent University-Corneel Heymanslaan, 10 (6B3), 9000 Ghent, Belgium

[2] Department of Plastic Surgery, University Hospital Gent, Ghent, Belgium

[3] Polymer Chemistry and Biomaterials Group, Department of Organic Chemistry, Faculty of Sciences, Ghent University, Krijgslaan, 9000 Ghent, Belgium

technologies regarding soft tissue deformities due to high patient expectations for improved functional/cosmetic outcomes [6]. Tissue engineering (TE) strategies are widely investigated to overcome the current surgical drawbacks.

3D bioprinting is a promising and popular branch of modular TE. 3D bioprinting has garnered immense interest over the last decade. The goal of bioprinting is to replace damaged tissues with live, vascularized, de novo created biosimilar constructs, suitable for surgical implantation. It promises to bridge the gap between artificially engineered tissue constructs and native tissues since it can co-deliver cells and biomaterials with precise control over the composition, spatial distribution, and architectural accuracy [7]. Computer software is able to extract data from patient images such as computed tomography scans or magnetic resonance imaging to produce tailor-made tissue implants. 3D culture models have been cited to overcome the gap between in vitro and animal studies in early-stage drug screening. In preclinical setting 95% of oncology drugs fail to receive FDA approval [8]. Part of the issue can be administered to the lack of suitable culture models that represent the in vivo environment. 3D culture models such as spheroids have proven to exhibit much more in vivo-like phenotype concerning cell metabolism and cell-cell interaction compared to any planar cell culture [9].

Spheroids or microtissues are cellular building blocks for fabricating a construct with a cellular organization. They can be compared to organoid structures encountered in embryology [10]. The organization of cells into a spheroid, or the fusion of spheroids into a macrotissue, is explained by the differential adhesion hypothesis (DAH). The DAH states that multicellular spheroids behave like liquids. Spheroids, consisting of motile cells, will rearrange and merge to maximize their adhesive bonds and minimize their free energy [11]. They can be stacked in a 3D composition to form larger constructs [12]. Experiments with tissue spheroids show that closely placed spheroids will fuse into larger microtissues [13]. This has been demonstrated by Jakab et al. [14], who placed two rounded embryonic heart cushion tissue explants in a hanging drop culture. These spheroids fused perfectly by fusion kinetics described for the fusion of two droplets [15]. Benefits of 3D spheroids over 2D monolayer cultures include increased adipogenic markers such as triglyceride accumulation as well as expression of adipose-specific genes such as peroxisome proliferator-activated-receptor-γ (PPAR-γ) [16]. Turner et al. [17] created a 3D spheroid model using human adipose-derived mesenchymal stem cells (ASCs) and their subsequent adipogenic differentiation in vitro. Mature ASC spheroids were evaluated based on functional markers such as CD36-expression and PPAR-γ gene expression. The authors report minimal spheroid loss during culture. The CD36-expression, representing cell competency for consuming extracellular fatty acids, was consistently found to be higher in 3D ASC spheroids compared to 2D monolayers. Such head-to-head comparison of 3D cultures vs 2D monolayer cultures may lead to a better in vitro model to uncover important biological mechanisms involved in diseases such as obesity and marks the importance of a 3D culture model in preclinical setting.

3D spheroids have been found to enhance pluripotent potential and differential efficacy of multiple mesenchymal cell lines when exposed to appropriate differentiation media in vitro [17, 18]. Kapur et al. [19] explored growth, composition and behavior of culture-expanded ASC spheroids using hanging-drop method. Their study demonstrates that ASC spheroids display a capacity for extensive renewal, developmental plasticity and internally directed organization. Their work confirms that ASC spheroids may be used to provide a flexible and practical modular foundation to build tissues and organs using bioprinting techniques.

Bioprinting relies on the use of a hydrogel as a cell-supporting matrix [20]. Hydrogels have become an attractive scaffold for TE purposes due to their ability to closely mimic the native tissue extracellular matrix (ECM) [6]. Various cell types such as adult cells, human umbilical vein endothelial cells (HUVECs), fibroblasts, cardiomyocytes, myoblasts, mesenchymal stem cells (MSCs), bone marrow-derived mesenchymal stem cells (BM-MSCs), neural stem cells (NSCs), ASCs, human induced pluripotent stem cells (iPSCs), glioma stem cells, and amniotic fluid-derived stem cells have been used for 3D bioprinting [21]. Despite good proofs of concept of appropriate matrices for bioprinting [22–24], the technology is still in its infancy and bioinks only recently became commercially available. Biomaterials such as alginate, fibrin, hyaluronic acid, silk, chitosan, decellularized ECM and pluronic F-127 have been used as scaffold material [25]. Collagen is one of the most abundant proteins present in the human body (around 30%) [26]. Yao et al. [27] encapsulated ASCs in collagen/alginate microspheres and after 4 weeks of culture, the spheres were macroscopically similar to AT lobules. After injection in mice, the authors observed vascularized AT constructs. It remains difficult to reproduce the delicate structure-function relationships of complex tissues and organs using this approach.

Van Vlierberghe et al. [28] noted that the desired scaffold for TE should have the modifiable mechanical properties of synthetic biomaterials and the biomimetic properties of naturally occurring biomaterials. Gelatin, a biopolymer formed by the hydrolysis of collagen, and its derivatives are some of the nature-derived bioinks that have gained significant attention. Generally, they have good biocompatibility, are cell supportive, biodegradable and easily optimized for bioprinting [25]. Vashi et al. [26] reported successful adipogenesis in mice after implanting a TE

chamber filled with gelatin microspheres impregnated with bFGF-2. An important limitation of natural biomaterials is their rapid rate of degradation upon contact with bodily fluids or culture media [29]. At low temperatures, gelatin forms a physical hydrogel network. In order to circumvent dissolution at 37 °C, methacrylamide-groups are incorporated into the gelatin. Gelatin-Methacrylamide (GelMA) is usually crosslinked with photoinitiators that allow to retain its biocompatibility with minimal cytotoxicity [30]. Long-term stability of the printed structure typically depends on the crosslinking mechanism after or during bioprinting. Irgacure® 2959 (Irg) is widely considered the golden standard for GelMA hydrogel crosslinking. Free radicals are created by the interaction of the photoinitiators with visible or UV light and initiate the polymerization reaction. This results in the formation of a stable chemically crosslinked gelatin network at physiological conditions after physical and chemical crosslinking [31]. GelMA is a cheap and easy to handle shear thinning biomaterial, which makes it suitable for extrusion-based printing methods. GelMA presents both natural cell binding motifs, such as RGD (Arg-Gly-Asp) and MMP-sensitive degradation sites, and different amino acid side-chain functionalities (carboxylic acid, amines, hydroxyl) which allow for further covalent modifications such as with hyaluronic acid [32]. Clevenger et al. [33] encapsulated ASCs in a biomimetic poly(ethylene) glycol (PEG) hydrogel with RGD cell attachment sequences along with MMP cleavage sites. ASC survival was supported, and the hydrogel demonstrated scaffold remodeling upon ASC differentiation, which potentially allows for greater vascularization of the graft through the holes created in the hydrogel scaffold through MMP cleavage. Huber et al. [34] encapsulated mature adipocytes in GelMA and was able to produce fatty tissue equivalents reaching similar tissue morphology to that of native fatty tissue after 14 days of culture. The authors proved that GelMA is a promising bioink for new printing techniques due to its biocompatibility and tunable properties.

The aim of the present work is to successfully fabricate high throughput adipogenic differentiated ASC spheroids and subsequently bioprint the ASC spheroids encapsulated in GelMA into a 3D construct for adipose tissue engineering (ATE). First, adipogenic differentiation of ASC spheroids was compared to a 2D culture. Second, ASCs and ASC spheroids were seeded on or encapsulated in GelMA. Finally, the encapsulated ASCs and ASC spheroids were 3D bioprinted. 3D bioprinting technology provides a potential solution for unmet clinical needs in breast reconstruction that builds on decades of experience and expertise in autologous fat grafting, ASC biology and TE. No studies, till now, have considered the use of bioprinting technology to fabricate AT constructs using predifferentiated ASC spheroids. The development of successful printing strategies requires investigation of all key elements in this process.

2 Materials and methods

2.1 Adipose-derived mesenchymal stem cell culture

ASCs (Cryo-Save, Niel, Belgium), characterized as $CD105^+$, $CD90^+$, $CD73^+$, $CD45^-$, $CD34^-$ (according to the International Federation for Adipose Therapeutics and the International Society for Cellular Therapy) by flow cytometry [35], were cultured in standard culture medium (SCM) consisting of Dulbecco's modified eagle's medium (DMEM) Glutamax (Gibco®, Life Technologies), supplemented with 10% fetal bovine serum (FBS) (Gibco®, Life Technologies), and 1% Penicillin/Streptomycin (Gibco®, Life Technologies) in T75 (75 cm^2) CELLSTAR™ Filter Cap Cell Culture Flasks (Greiner Bio-One GmbH, Germany, Cat. No. 82050-856) at a density of 350,000–500,000 cells per falcon as previously described [35, 36]. The falcons were placed and maintained in a humidified 5% CO_2-containing atmosphere at 37 °C. Culture medium was replenished twice a week. Once 80–90% confluency was achieved, ASCs were dissociated from the culture flasks with TrypLE® (Gibco®, Life Technologies). Adipogenic differentiation medium (ADM) consists of SCM supplemented with 1 µM dexamethasone (Sigma-Aldrich®, D4902), 200 µM indomethacin (Sigma-Aldrich®, I7378), 10 µg/mL insulin (Sigma-Aldrich®, I9278), 0.5 mM 3-isobutyl-1-methylxantine (IBMX) (Sigma-Aldrich®, I5879). All cell types were used up to passage 10 and were cultured at 37 °C in a humidified 5% CO_2-containing atmosphere.

2.2 Microchip fabrication, spheroid formation and collection

Spheroids were generated by using a non-adherent microwell culture system, as previously described [37, 38]. Tailor-made, negative polydimethylsiloxane (PDMS) microchip molds have a diameter of 1.8 cm and generate a microchip with 2865 pores with a diameter of 200 µm consisting of Ultrapure™ Agarose (Life Technologies) 3 w/v%. In total, 10^6 ASCs in 0.5 mL SCM were seeded per microchip to obtain spheroids [39]. After 24 h, SCM was removed and replenished with ADM. The morphology of the spheroids was analyzed through observation utilizing phase-contrast microscopy (Olympus IX 81). The evaluation of the morphometry was performed using the Xcellence image software that allowed the determination of several parameters, such as diameter, perimeter (p), and area (A).

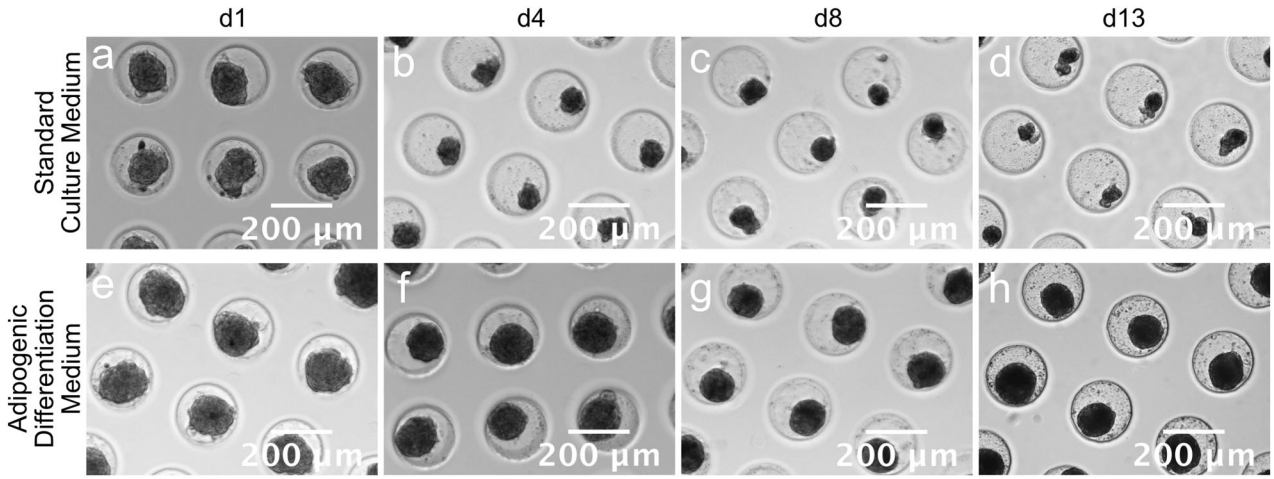

Figure 1 Phase contrast images (×10) of spheroids cultured in SCM (**a**–**d**) and spheroids cultured in ADM (**e**, **f**) on day 1, 4, 8 and 13

The formula $f_{\text{circularity}} = (4\pi A)/p^2$ enabled the ability to calculate the circularity of the spheroids. For diameter and circularity evaluation, phase-contrast images of 75 spheroids cultured in SCM or ADM (illustrated in Fig. 1), derived from three independent experiments ($n = 3$), were assessed at 1, 4, 8 and 13 days. Spheroids were harvested at 1, 4, 8 and 13 days from the microchips in their respective medium, collected in a tube, and centrifuged to obtain a spheroid pellet and further analyzed with phase contrast microscopy, fluorescence microscopy, histology and q-RT-PCR as described below. For 3D hydrogel and bioprinting experiments, spheroids were collected after 3 days and encapsulated in GelMA subsequently.

2.3 2D GelMA hydrogel evaluation

2.3.1 2D adipogenic differentiation on GelMA hydrogels

GelMA, provided by the Polymer Chemistry and Biomaterials group (UGent), with a degree of substitution of 95% (DS95) was sterilized with ethylene oxide (cold cycle, AZ Sint-Jan, Brugge) and dissolved in PBS at 37 °C to obtain a 10 w/v% solution. 1-[4-(2-Hydroxyethoxy)-phenyl]-2-hydroxy-2-methyl-1-propane-1-one, also known as Irg (Ciba® Specialty Chemicals, Basel, Switzerland), was made to a concentration of 0.8 w/v% in PBS and mixed with GelMA according to the formula below.

$$\text{The amount (in mL) of Irg (2 mol\%) needed for one gram of GelMA} = 0.000385\ (\text{mole amine functions for 1g of GelMA}) \times 0.95\ (\text{DS\%}) \times 0.02\ (2\ \text{mol \% Irgacure 2959}) \times \frac{224.3\ (\text{Molecular weight of Irgacure 2959})}{0.008\ (0.8\ \text{wv\% concentration of Irgacure 2959})}$$

Hydrogel discs were prepared by pipetting 250 µl GelMA solution in each well of a 48-well plate and crosslinked for 20 min with 365 nm UV-A light (4 mW/cm², UVP Inc.) in the presence of 2 mol% Irg.

In total, 20,000 ASCs in 0.5 mL SCM were seeded on 48-Multiwell Plates (21,053 ASCs/cm^2) containing the hydrogels. As control, ASCs were seeded with a density of 40,000 cells/well in 24-well plates (21,053 ASCs/cm^2). After 48 h, SCM or ADM was added to the wells. Differentiation was observed at day 7, 11 and 14. ASCs were analyzed with fluorescence microcopy and q-RT-PCR as described below.

2.3.2 Encapsulation of ASCs and spheroids in GelMA

GelMA DS95 was prepared and mixed with Irg as described in "2D adipogenic differentiation on GelMA hydrogels". ASCs were resuspended in the GelMA/Irg-solution at a concentration of 10^6 ASCs 250 µL^{-1}. Spheroids were suspended in the GelMA/Irg-solution at a concentration of 1 microchip (10^6 ASCs) 250 µL^{-1}. The 250 µL-suspensions were added to 48 multiwell plates. After physical gelation of 30 min at 4 °C, the solution was illuminated for 15 min with UV-A (365 nm, 8 mW cm^{-2}, UVP Inc.) in a laminar flow cabinet with a TFL-40V transilluminator (UVP 95042001, Thermo Fisher Scientific Inc.). Constructs were cultured in ADM. Analyses were conducted on day 7, 11, 14 and 23.

2.4 Bioprinting

3D bioprinting was performed with the 3DDiscovery® (RegenHU LTD) using a time pressure-based printhead. Printing parameters such as printing pressure, printing temperature, needle geometry and diameter, feedrate, as well as the mechanical properties of the bioink will influence the thickness of the strands. 3D models can be

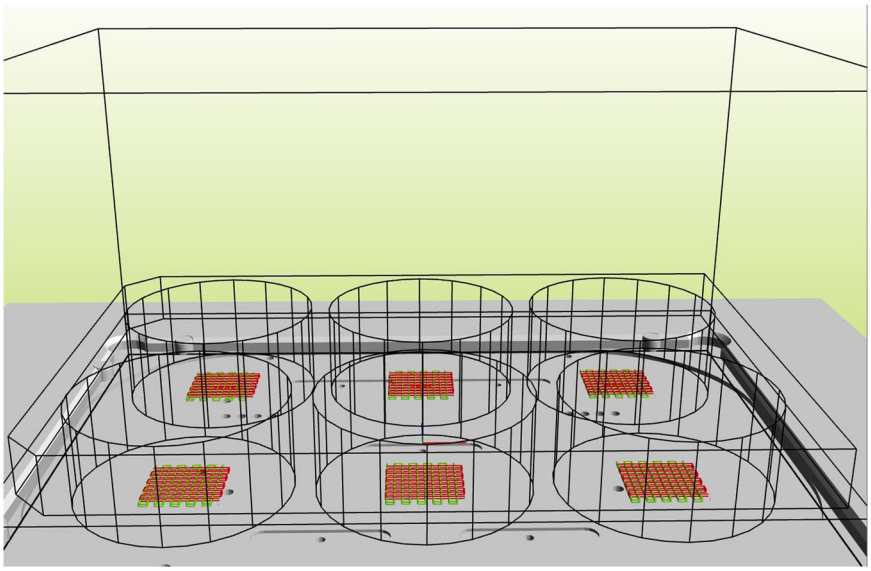

Figure 2 BioCADTM software 3D image of the design. Scaffolds with ten struts and four layers in six-well plates

designed layer-by-layer with BioCAD™, a drawing suite enabling us to design a scaffold from scratch (as seen in Fig. 2). The BioCAM™ software then generates a toolpath based on the 3D digital models acquired from the BioCAD™ software.

ASCs and spheroids were encapsulated in GelMA at a concentration of respectively 4×10^6 cells mL^{-1} and 4 microchips mL^{-1}. The single cell or spheroid-laden GelMA is placed in the cartridge heater (23 °C). Four layers were printed (Fig. 2). Each layer consists of ten struts. A conical needle with gauge 25 (ID of 0.25 mm) was used to print, which resulted in constructs with a height of ±1 mm. The constructs are made of layers with dimensions of 13 × 13 mm and a line space of 1 mm.

After printing at 5 mm s^{-1}, the constructs undergo physical gelation (30 min at 4 °C) before being crosslinked under the same conditions as previously mentioned. To intensify cross-linking, immersion fluid, consisting of PBS with photoinitiator in equal concentration as the GelMA-solution, was added. After crosslinking, the structures are rinsed with PBS and submerged in appropriate medium and placed in an incubator at 37 °C and 5% CO_2.

2.5 Analyses and assays

2.5.1 Live/dead assay

A live/dead viability assay was conducted with Calcein AM (CA) (cell-permeant dye, Anaspec, AS-89201) and propidium iodide (PI) (Sigma-Aldrich®, P4170) to measure the viability of ASCs and spheroids. Pictures were made using an inverted fluorescence microscope (Olympus IX 81) with filters for green fluorescent protein (GFP) and Texas Red (TxRed). The microscope is equipped with Xcellence software (Olympus).

Confocal images were captured with a Nikon A1R inverted confocal microscope with a dry objective (×10) and NIS Elements Viewer software (Nikon Instruments B.V.). EGFP laser (488 nm) and TxRed laser (561 nm) were selected. ND2-files were imported in (Fiji is just) Image J for analysis.

2.5.2 Oil Red O

Oil Red O staining was performed on 2D differentiation and spheroid experiments. ASCs or spheroids were rinsed with PBS and fixed with 4% NBF (neutral buffered formaldehyde). After rinsing with distilled water, dehydrating with 60% Isopropanol and staining with Oil Red O, the cells could be visualized with light microscopy (Olympus IX 81).

2.5.3 Hematoxylin–eosin staining

Spheroids were fixed with 4% NBF overnight after 14 days of culture. The spheroids were passed through decreasing alcohol concentrations (100, 90, 80, 70%) and embedded in paraffin to obtain 5 µm coupes with a microtome. The sections were colored with HE and evaluated with light microscopy (Olympus BX51).

2.5.4 OsO4 staining and transmission electron microscopy

Spheroids were fixed with 2% glutaraldehyde after 14 days of culture. Glutaraldehyde was replaced with cacodylate buffer after 1 h. The buffer was replaced by osmiumtetraoxide for 90 min and again replaced by cacodylate buffer. Afterwards, increasing acetone concentrations were added to the spheroids to be finally embedded in Spurr kit (Sigma). Semi-thin sections of 1 µm were mounted,

counterstained with hematoxylin–eosin and analyzed with light microscopy.

Thin sections (60 nm) were cut, stained with uranyl acetate and lead citrate and examined using a JEOL 1200 EX II transmission electron microscope operating at 80 keV [36, 40].

2.5.5 Gene expression analysis (RT-qPCR)

To evaluate adipogenic differentiation, TaqMan gene expression assays (Applied Biosystems, Foster City, California) were performed for PPAR-γ and fatty acid binding protein 4 (FABP-4) on day 7 after encapsulating spheroids or bioprinting. PPAR-γ is a member of the nuclear-receptor superfamily and a regulator of adipocyte differentiation [41]. FABP-4 is a late marker of differentiation, encoding the fatty acid binding protein found in adipocytes, and its roles are believed to include fatty acid uptake, transport, and metabolism [42]. Total RNA was extracted from cells using Trizol (Qiagen, Vento, The Netherlands), and treated with DNAse I (Invitrogen). Concentration and purity of RNA was measured using spectrophotometry, after which reverse transcriptase reaction was performed using a universal reverse transcriptase kit (Eurogentec, Liege, Belgium) according to the company's protocol. Reverse transcriptase–quantitative polymerase chain reaction was performed for gene expression analysis on the 7500 Fast Real Time Polymerase Chain Reaction System (Applied Biosystems, Foster City, Calif.). Relative quantification (n-fold expression) values were calculated using the equation $2^{-\Delta\Delta Ct}$ relative to control ASCs at day 0. GAPDH (4326317E-0906030) was selected as endogenous control.

2.5.6 Confocal images and Image J

To investigate the impact of 3D bioprinting on viability, scaffolds containing encapsulated spheroids were compared with 3D bioprinted spheroid scaffolds ($n = 30$) through confocal images (Nikon A1R inverted confocal microscope) after 7 days of culture in ADM. Spheroids were fabricated and encapsulated in GelMA as stated above. Scaffolds were 3D bioprinted under the same conditions as stated in 3.4. CA/PI was added to the encapsulated spheroids and printed scaffolds and incubated for 30 min. Confocal images were taken by a Nikon A1R inverted confocal microscope with NIS Elements AR software. 10 µm coupes were taken at random points to give a full image-depth at a certain point. The ND2-files were imported in (Fiji is just) Image J software. Viability was measured according to standard protocol by Bioactive Regenerative Therapeutics, Inc. Channels were split in red and green channels, converted to 8-bit and projected in one focal plane. Intensities were measured and quantified.

2.6 Statistics

All analyses represent data from three independent experiments. Data were analyzed using SPSS version 24.0 (SPSS GmbH Software) and are presented in the form of mean ± SD. To test for normality of the variables, the Shapiro–Wilk test was performed. The homogeneity of variances was assessed using the Levene's test. A student's t test was used to determine significant differences in sphericity and diameter between spheroids cultured in ADM and spheroids cultured in SCM on day 1, 4, 8 and 13. The difference in mean survival after 7 days of culture of spheroids encapsulated in GelMA vs spheroids bioprinted after encapsulation in GelMA was determined using a student's t test. To indicate the equivalent differentiation rates in both study groups, tested with the differentiation assay, a Mann–Whitney U test was performed. Statistical significance was considered to be a p value less than 0.05.

3 Results

3.1 Biofabrication of adipose-derived mesenchymal stem cell spheroids

Spheroids were formed by seeding 1,000,000 ASCs on each agarose microchip with 200 µm pores in presence of SCM. Each agarose microchip has 2865 pores of 200 µm diameter, thus one microwell contains ~349 cells which will form one spheroid. Within 24 h after seeding, the ASCs formed spheroids and SCM was replenished with ADM (Fig. 1e) and compared to spheroids cultured in SCM (Fig. 1a) for 13 days.

Spheroid geometry was characterized by measuring the diameter and circularity. Evaluation of the diameter of the spheroids cultured in SCM after 1, 4, 8 and 13 days showed significant smaller spheroids compared to spheroids cultured in ADM over time. The spheroids cultured in SCM decreased from a diameter of 134 ± 9.92 µm on day 1 to a diameter of 68 ± 4.63 µm on day 13. Spheroids cultured in ADM also decreased over time, albeit less significantly than the SCM group. On day 1 the average diameter was 153 ± 9.18 µm and decreased to 101 ± 5.70 µm on day 13. Both groups showed compaction during the entire experiment but more pronounced in the SCM group (Fig. 1e). After 8 days, the diameter is maintained in both groups (Fig. 3). Spheroids cultured in SCM were less uniform, smaller, more polygonal in shape and prone to disintegrate over time, associated with a higher amount of cell debris (Fig. 1d). Spheroids cultured in ADM have a significantly larger diameter ($p < 0.001$ with Student's t comparison) compared to spheroids cultured in control medium on day 1 (19.16 µm CI: [13.75; 24.58]), 4 (45.5 µm CI: [41.9; 49.0]), 8 (30.5 µm CI: [28.2; 32.9]) and 13 (32.8 µm CI: [29.8; 35.7]).

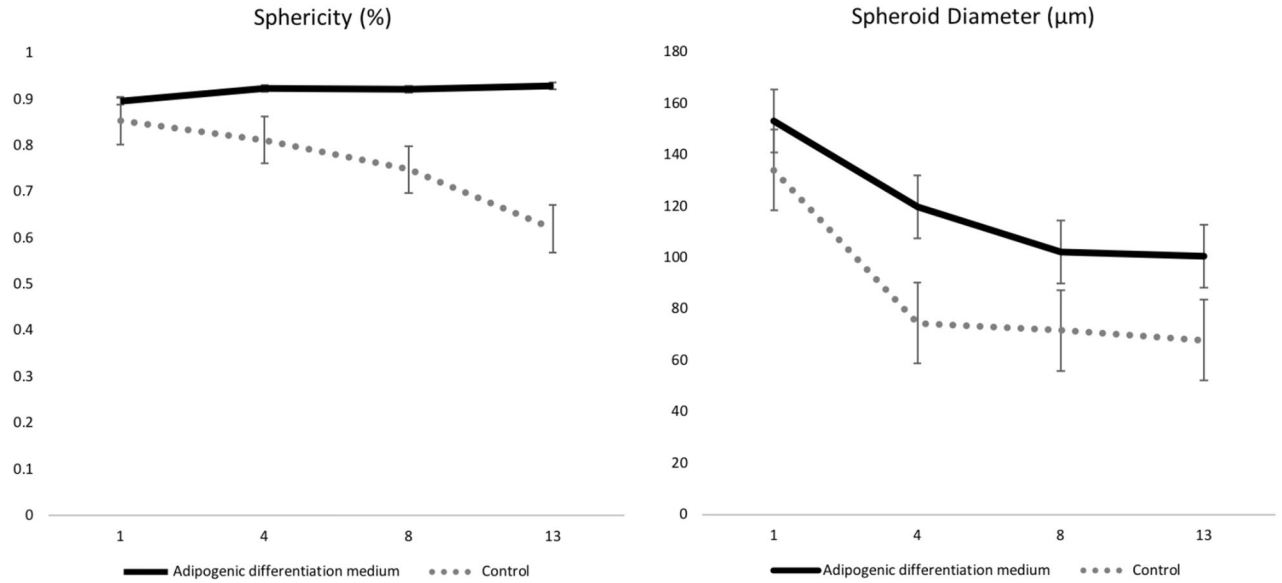

Figure 3 Sphericity and diameter of spheroids cultured in ADM or SCM at 1, 4, 8 and 13 days. Spheroids cultured in ADM are significantly more circular and have a larger diameter compared to spheroids cultured in control medium at each day ($p < 0.001$, with Student's t comparison). Bar graphs represent standard deviation

Spheroids cultured in SCM lost their round shape over time (Fig. 1a). On the last day, the round shape could not be seen in the control group anymore. This is confirmed by measuring the circularity, which is calculated by the formula $4\pi \frac{\text{Area}}{\text{Perimeter}^2}$. A value of 1 indicates a perfect circle. Spheroids cultured in ADM are significantly more circular ($p < 0.001$ with Student's t comparison) at day 4 (11.1% CI: [0.089; 0.134]), 8 (17.3% CI: [0.143; 0.203]) and 13 (30.8% CI: [0.274; 0.342]). Circularity remained stable >90% in the ADM group. Circularity slightly increased from day 1 to day 13 for the adipogenic differentiation group, correlating with the decrease in diameter and showing compactness.

The morphology and differentiation capacity of ASC spheroids was analyzed with different methods: Oil Red O, HE, OsO4 (light microscopy and electron microscopy) as seen in Figs. 4 and 5. Oil Red O staining showed a more intense and uniform staining of lipid droplets compared to control. HE staining of spheroids in adipogenic culture medium showed cavities that might indicate lipid droplets since lipids dissolved in alcohol upon staining (Fig. 4, HE, black arrow). This is in contrast to spheroids in SCM which showed no cavities. Upon fixation with glutaraldehyde and OsO_4 on day 13, intracellular lipid droplets were visualized in spheroids cultured in ADM. Spheroids cultured in SCM showed minuscule lipid droplets, indicating less differentiation. Electron microscopy analysis (Fig. 5) confirmed the presence of giant lipid droplets and collagen III (one of the main constituents of the interstitial matrix, secreted by adipogenically differentiated cells) deposition in spheroids cultured in ADM.

3.2 Compatibility of single cells with GelMA

Single cells seeded on GelMA hydrogels (Fig. 6a) showed good viability in both the adipose group and the control group. Up to 14 days after seeding the ASCs on GelMA, a high viability was seen. The ASCs cultured in adipogenic differentiation medium showed a polyhedral morphology with multiple vacuoles. Cells in SCM expressed a more fibroblast-like morphology with minimal differentiation. This form was maintained with minimal increase of minuscule lipid droplets by day 14. Upon Oil Red O staining, differentiation was significantly higher compared to controls, which retained a spindle shape. A multivacuolar morphology, filling the cytoplasm, was seen after 14 days of culturing. In the control groups, almost no Oil Red O staining could be seen.

After 14 days, vacuoles with lipids could be observed in encapsulated single cells in GelMA (Fig. 6, g). Even after 14 days we had perfect viability in the adipose group, in which the adipocytes showed a typical polyhedral morphology. Since cells are embedded in 3D, the microenvironment is more related to natural AT. Up to 23 days after encapsulating the ASCs in GelMA, a high viability was seen.

3.3 3D printing of ASCs/spheroids encapsulated in GelMA

Constructs were 3D printed with a time-pressure printhead (DD-135N) at RT (19 °C) with a cartridge heater

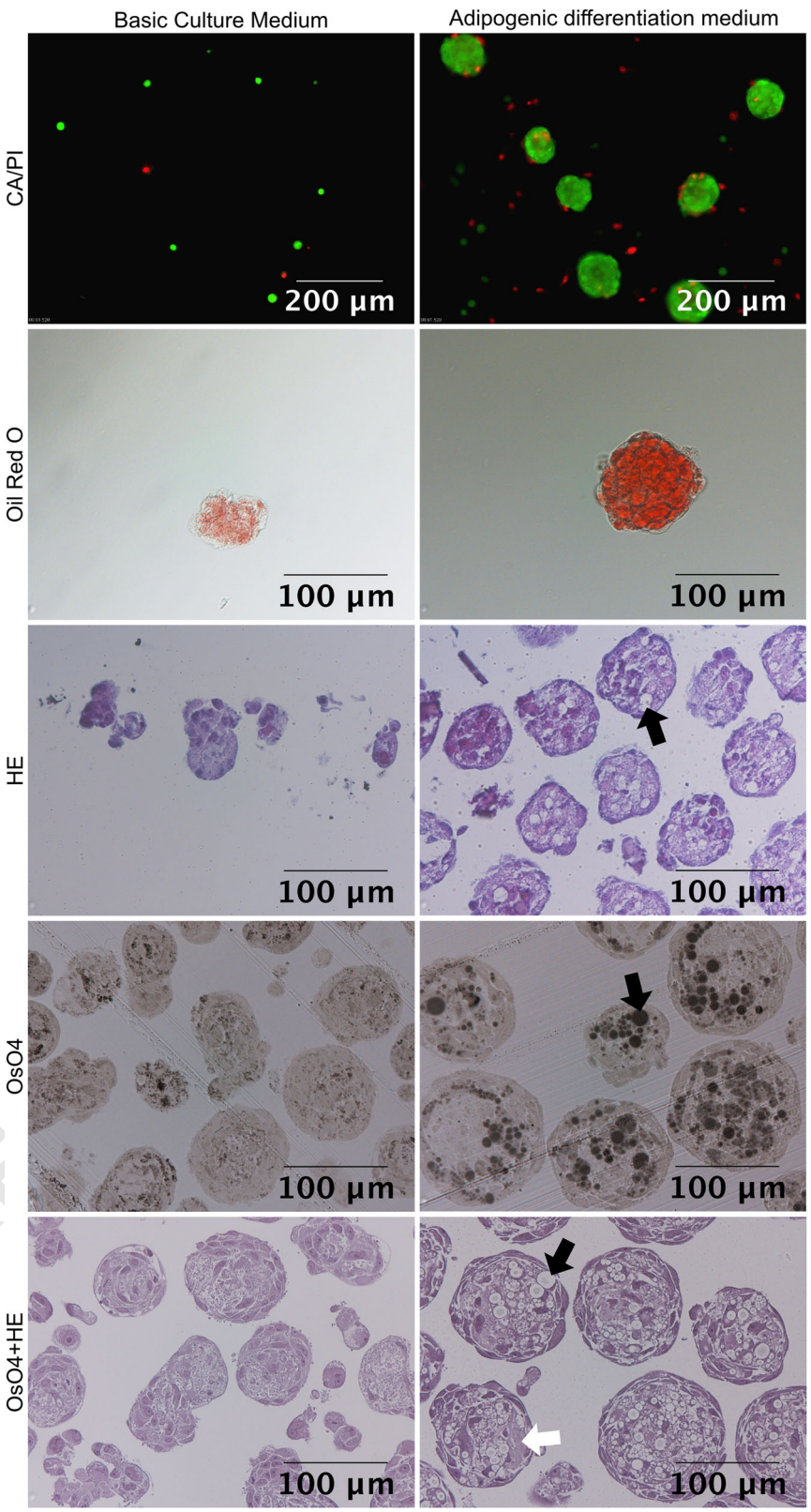

Figure 4 Viability analysis with Ca/PI and differentiation analysis with Oil Red O, HE, OsO4 fixation (light microscopy, HE) after 7 days. Spheroids were cultured in SCM or ADM. Ca/PI staining was analyzed with fluorescence microscopy, differentiation was analyzed with light microscopy. White arrow: amorphous zone. Black arrow: lipid droplet

(CF-300H) set to 23 °C. The 3DDiscovery© was set to a feedrate setting (5 mm s^{-1}). Printing took around 15 min to complete a six-well plate with squared scaffolds of 13 and 1 mm high (Fig. 7). After physical gelation at 4 °C for 30 min, the constructs were illuminated under UV light (365 nm) at 8 mW cm^{-2} for 15 min in immersion fluid, to

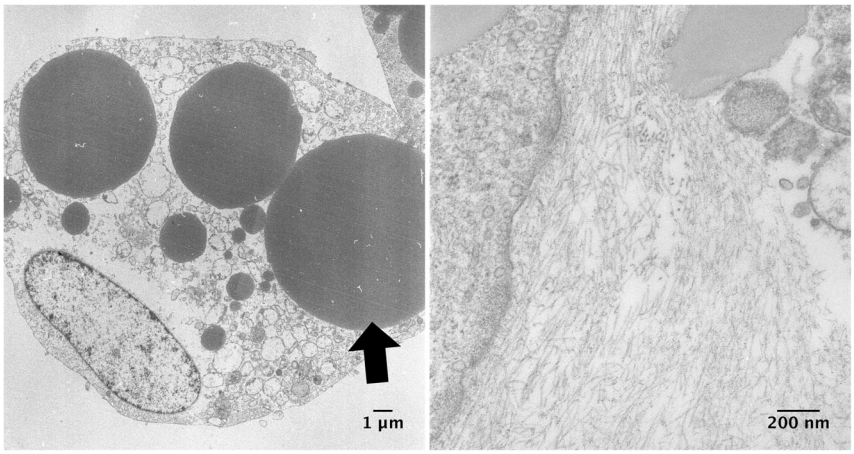

Figure 5 Adipogenic differentiation of spheroids cultured in ADM after 7 days. Visualization of cell morphology (left picture) and deposition of extracellular structures (collagen III, right picture). Black arrow: lipid droplet. Transmission electron microscopy

counter dissolution of the scaffolds at 37 °C due to inefficient crosslinking of GelMA. After photocrosslinking, the immersion fluid was removed, the constructs were rinsed with PBS and ADM or SCM (control) was added. The constructs were incubated at 37 °C and 5% CO_2.

In total, 95% of the scaffolds were intact after 24 h at 37 °C. Viability was good in both the adipose group as in the control groups (Fig. 7). As seen in all pictures, a homogenous distribution of cells was obtained. Equal viability was observed at the edges of struts as at the center of struts. Almost no dead cells were observed after 7 days of culture. In the spheroid group, a heterogeneous solution for printing was obtained. Spheroids were homogeneously distributed in the GelMA bioink as well as in the printed GelMA scaffold. Typical adipocyte features such as univacuolar morphology, or a grid structure cannot be observed within 7 days of culture (Fig. 8).

No significant difference was found in viability between spheroids encapsulated in GelMA (80% ± 0.086) and spheroids encapsulated in GelMA and subsequently bioprinted (79% ± 0.078) after 7 days of culture ($p > 0.05$ and $n = 30$). Obtained images through CLSM are illustrated in Fig. 9.

In TE, microtissues are used as building blocks for the assembly of larger tissue constructs. Giant cell clusters were noticed in the gel 7 days post-printing the scaffolds (Fig. 9).

3.4 RT-qPCR

To assess adipogenic differentiation, upregulation of key adipogenic marker genes was detected at transcriptional level (Fig. 10). PPAR-γ and FABP-4 mRNA levels were quantified after 7 days of culture in ADM using RT-qPCR. As negative control sample, ASCs cultured in standard culture medium for 7 days, was used for comparison. An upregulation of the adipogenic specific genes was observed in spheroids cultured in microchips in ADM (Sphe), spheroids encapsulated in GelMA and cultured in ADM (GM Sphe) and spheroids encapsulated in GelMA and subsequently bioprinted (Print Sphe). mRNA levels of FABP-4 were five times higher and PPAR-γ levels were twice as high compared to the control sample. No significant difference in gene expression was found when comparing the different spheroid conditions. A clear trend in upregulation of both genes is seen in all spheroid conditions compared to positive control consisting of ASCs cultured in adipogenic culture medium for 7 days.

4 Discussion

Classic top down TE approaches originate from attempts by chemical engineers to create porous scaffolds from biodegradable polymers as a temporary template that supports cell attachment and tissue neomorphogenesis [43]. This approach is hindered by limited control over cell–cell contact and microarchitecture [44]. In the context of modular bottom-up TE, spheroids are used as micro-building blocks for the fabrication of a macrotissue. In the present study, we developed a method to bioprint viable ASC spheroids, encapsulated in GelMA, in a desired 3D configuration. The use of a 3D bioprinter enables us to assemble these building blocks layer-by-layer with high spatial control.

ASCs have become the focus in many TE strategies. The abundantly availability of AT and its inherent regenerative potential allows patients to donate a sufficient quantity for cell isolation with minimal risk of adverse effects. They are abundantly available, easy to harvest, multipotent and less painful to extract than BM-MSCs. They can easily be extracted after small liposuction under local anesthesia. AT possesses superior stem cell content compared to other tissues; as much as 2% of the cellular content of adipose may be ASCs, compared to 0.002% BM-MSCs in bone marrow [17]. ASCs cultured in vitro in the form of 3D spheroids have improved viability, self-renewal capacity,

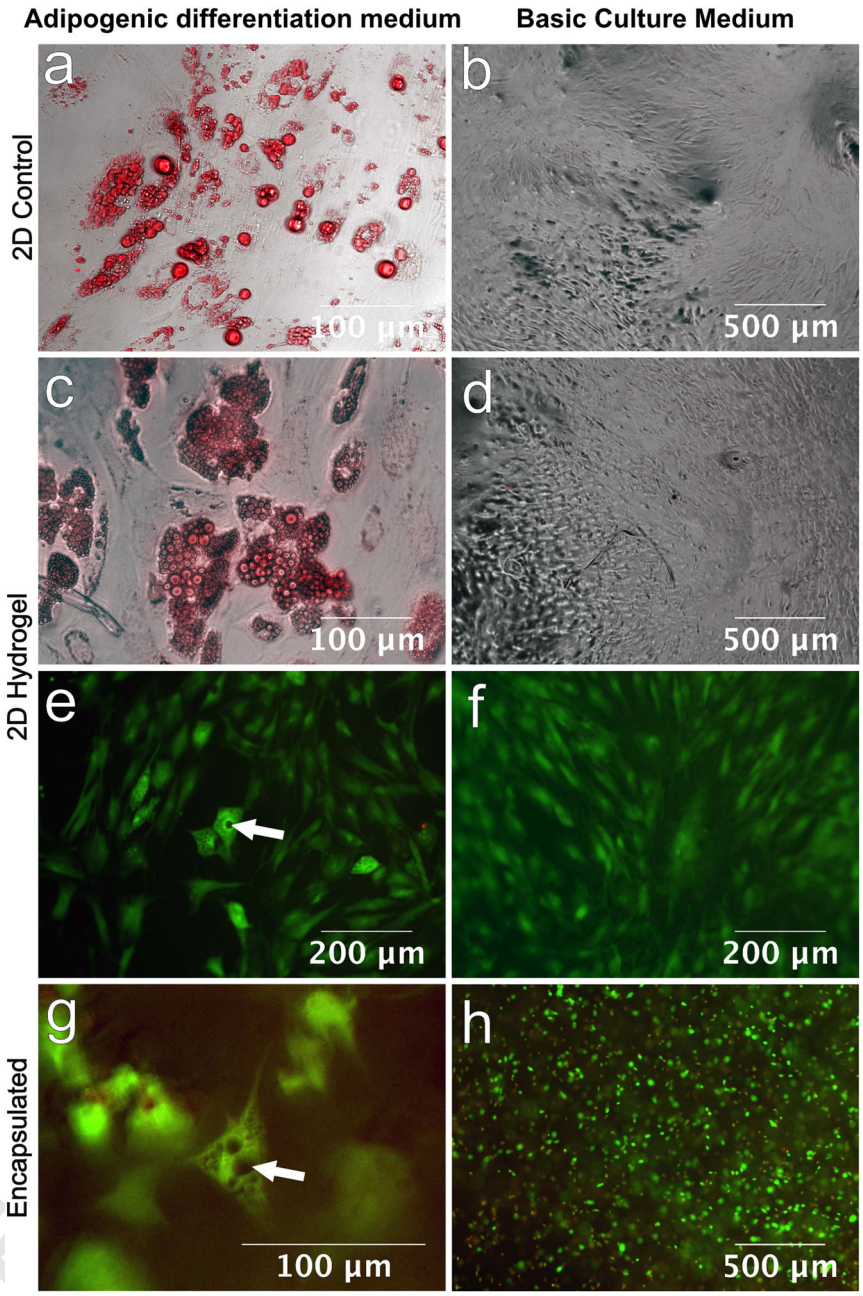

Figure 6 **a–d** ASCs seeded on GelMA: 20,000 ASCs were seeded on GelMA films and cultured in control or adipogenic differentiation medium. Oil Red O staining at 14 days taken with a combination of Brightfield and TxRed filters. **e–h** ASC encapsulation in GelMA 10 w/v%, 10^6 ASCs mL^{-1}. Pictures taken at 14 days. All pictures are live/dead assays taken with GFP filters. White arrow: lipid droplets

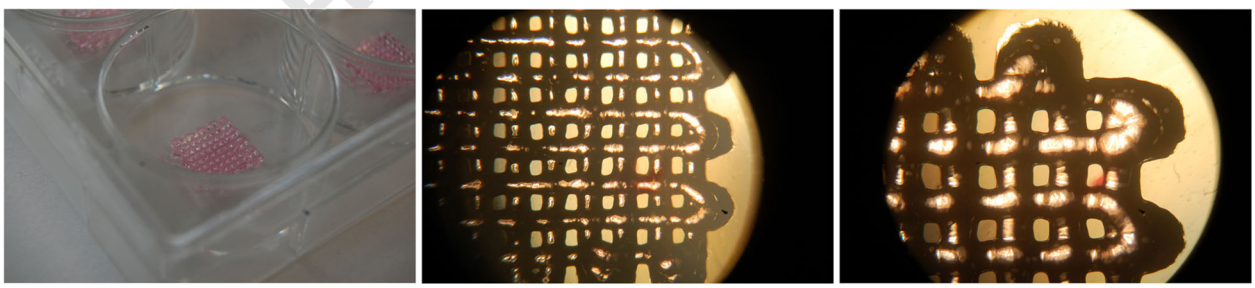

Figure 7 Bioprinted scaffolds measure 13 × 13 × 1 mm. Pictures of constructs taken after physical gelation at 4 °C for 30 min and illuminated under UV light (365 nm) at 8 mW cm^{-2} for 15 min in immersion fluid

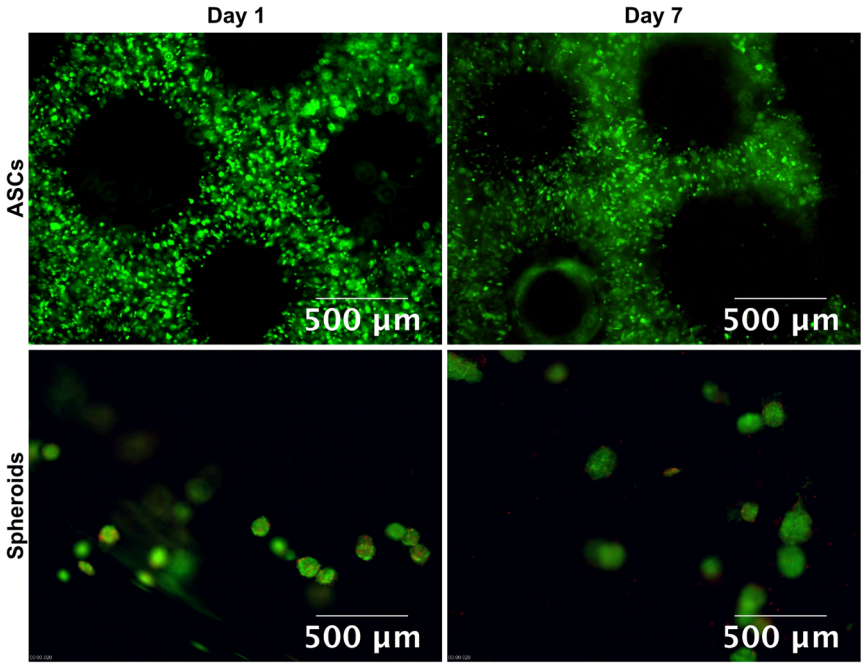

Figure 8 Bioprinting ASCs or spheroids encapsulated in GelMA. ASCs (superior row) or spheroids (inferior row) encapsulated in GelMA cultured in ADM. Pictures are live/dead assays at day 1 and 7 post-printing (Olympus IX 81). A good viability was observed after 1 and 7 days. A slight decline in viability was observed after 7 days in encapsulated ASCs

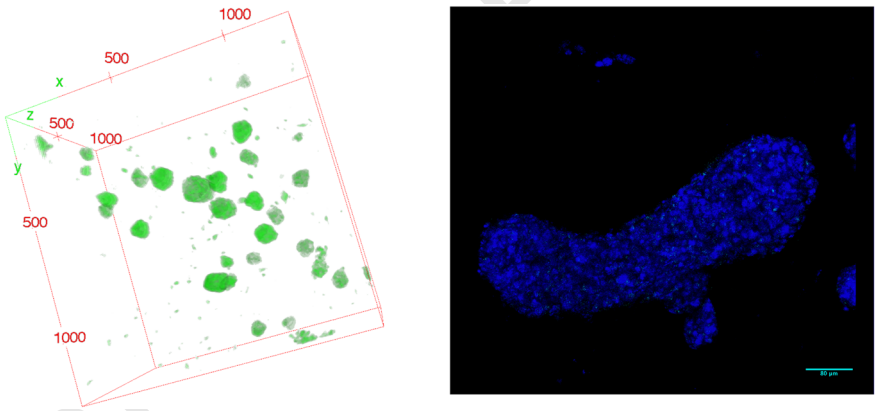

Figure 9 Left: confocal images taken with Nikon A1R inverted confocal microscope and projected in 1 focal plane using (Fiji is just) Image J software. Picture is taken 7 days post printing. Right: giant cell cluster 7 days post-printing spheroids in GelMA. Picture taken with Nikon A1R inverted confocal microscope

and differentiation potential compared to 2D-cultured cells as seen in our experiments. A number of studies have demonstrated that 3D bioprinting ASC single cells is not cytotoxic and preserves proliferative and adipogenic differentiation capabilities of non-printed ASCs [34]. This is confirmed in our research: both encapsulated and printed ASC spheroids show excellent viability. ASCs seeded on or encapsulated in GelMA show a polyhedral morphology with multilocular microvacuoles within the cell cytoplasm, which are morphological features associated with immature adipocytes.

To demonstrate the successful differentiation and long-term maintenance of the 3D human adipose stem cell spheroids as functional adipocytes, we analyzed expression of PPAR-γ, a key gene involved in adipogenesis, using RT-qPCR. An upregulation of the adipogenic specific genes was observed in spheroids encapsulated in GelMA and subsequently bioprinted. mRNA levels of FABP-4 were five times higher and PPAR-γ levels were twice as high compared to the 2D control sample. These findings are consistent with a recent experiment of Kim et al. [45] who encapsulated ASC spheroids in an alginate solution and subsequently bioprinted the mixture. They measured PPAR-γ levels 4.40-fold higher than control samples. Turner et al. [17] measured 2–5-fold PPAR-γ expression in ASC spheroids cultured in ADM compared to 2D monolayer cultures. In the adipogenic differentiation process, several parameters can enhance the differentiation: (1) the adipogenic culture medium, (2) the cellular environment (2D cell monolayers vs 3D spheroids), (3) the hydrogel (cells or spheroids encapsulated in the hydrogel) and (4) the hydrogel processing (encapsulation or bioprinting). In the present work, we have analyzed the adipogenic expression after 7 days. At that time point, the adipogenic culture medium

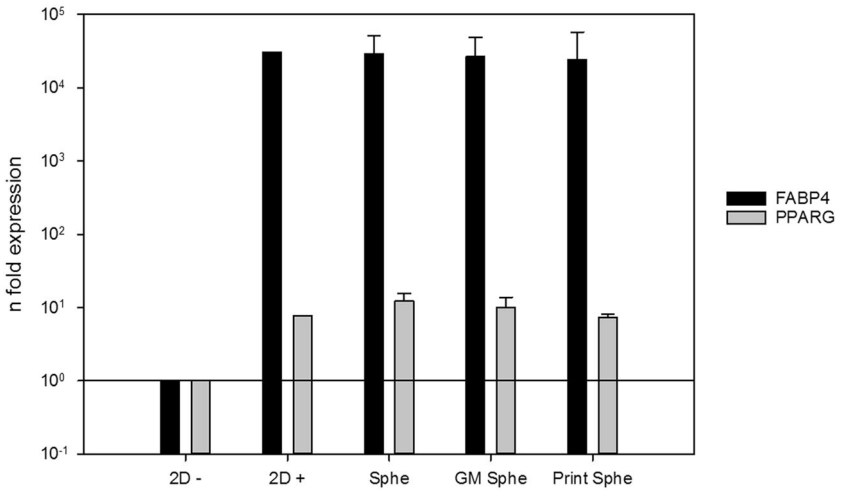

Figure 10 Real-time quantitative polymerase chain reaction analysis of the gene expression of adipogenic markers FABP-4 and PPAR-γ. 2D negative control: ASCs cultured in SCM (2D−) ($n = 1$), 2D positive control: ASCs cultured in ADM (2D+) ($n = 1$), Spheroids cultured in microchips in ADM (Sphe) ($n = 3$), Spheroids encapsulated in GelMA and cultured in ADM (GM Sphe) ($n = 3$) and spheroids encapsulated in GelMA and subsequently bioprinted (Print Sphe) ($n = 2$). PPAR-γ and FABP-4 mRNA was measured after 7 days of culture. Bar graphs represent the logarithmic normalized fold expression relative to control ASCs (2D−) on day 0. Values are the mean fold change & SEM of n replicate experiments; $*p > 0.05$ with Mann–Whitney U test

still have the largest influence on the adipogenic differentiation. The other parameters (spheroid formation, hydrogel and bioprinting) will definitely have an impact on adipogenic differentiation but this can only be notified at other time points. We believe that adipogenic differentiation will be enhanced in spheroids compared to 2D monolayers at very early time points due to cell–cell interactions. At later time points, it will be expected that the differentiation in cellular spheroids can be more homogeneous. Importantly, current experiments have been performed with GelMA as bioink. In the future, other bioinks with improved impact on adipogenic differentiation will be developed. These are the reasons why 3D bioprinting did not have a huge impact on adipogenic differentiation, nevertheless, the adipogenic differentiation did show a small increase compared to cells cultured as 2D monolayers.

We are able to conclude that ASCs lose their proliferative capability as seen in our sphericity measurements: decrease in diameter until an equilibrium is reached. Spheroids gradually exhibit behaviors associated with AT such as triglyceride accumulation and expression of adipogenic genes and transcription factors. In addition, ASC spheroids vastly outperformed 2D monolayer cultures regarding CD36 and PPAR-γ-expression due to contact-inhibited proliferation which serves as a cue for enhanced adipogenic differentiation [17]. A clear trend in upregulation of both FABP-4 and PPAR-γ is seen in all spheroid conditions compared to positive control consisting of ASCs cultured in adipogenic culture medium for 7 days in our experiments. This indicates differentiation toward mature adipocytes in bioprinted constructs. We measured spheroid clusters of almost 600 µm, which is way more than the 200 µm fabricated spheroids. The bioprinting needle has an internal diameter of 0.25 mm in order to obtain higher resolutions. This leads to the hypothesis that clusters were formed after printing through tissue fusion, indicating tissue formation. In addition, they showed reasonable viability upon live/dead staining. Autonomous self-assembly TE such as spheroids is based on embryological processes of tissue development [28]. Our experiments showed no significant difference in gene expression comparing the different spheroid conditions, marking the negligible influence of bioprinting on differentiation capacity in addition to excellent viability.

Live/dead assays of the bioprinted constructs show a mean viability of 79% ± 0078 after 7 days of culture ($n =$ 30). Until now, no other research group has bioprinted ASC spheroids in GelMA. Single ASCs have been encapsulated in multiple experiments and show viabilities in the same range [46]. Huber et al. [34] incorporated mature adipocytes in methacrylated gelatin for ATE and measured its mechanical properties. The authors mention storage moduli similar to native AT when small forces (0.05 N) are applied. Under higher loads (0.5 N), the storage modulus of native AT was significantly higher than methacrylated gelatin. Natural AT is organized in lobules containing adipocytes, surrounded by connective tissue. Hence the big difference in storage moduli between low and high loads. Evidence shows that mechanical properties of a scaffold can influence the differentiation of mesenchymal stem cells to a specific lineage [6]. ASCs tend to differentiate toward an adipogenic

cell type when seeded onto a softer scaffold [47]. It is difficult to engineer a bioink that features the variable mechanical properties of a tissue and the anatomical relations of the different cell types. A bioink is only a temporary scaffold that will be replaced by self-made ECM after cells undergo self-assembly and self-organization.

We only used a 10 w/v% hydrogel because of its excellent bioprinting properties, which is consistent with the work of Huber et al. [34], who concluded that non-cured GM in solution is cytocompatible with mature adipocytes in the tested range of 0.6–10 w/v%. In our protocol GelMA was illuminated up to 15 min in order to prevent dissolution at 37 °C post-printing. This is significantly more than the curing times of up to 1 min by Gungor-Ozkerim et al. [48]. Still, we managed to have a mean viability of 79%. Irg is the most commonly used photoinitiator but its peak absorption point is not optimal to work with living cells. The excitation peak is around 279 nm. When working with cells, higher wavelengths (365–400 nm) are used because 279 nm would likely cause DNA damage and protein damage. The absorption peak of VA-086® is ~385 nm, which is in the UV-A range and has been shown to have excellent biocompatibility properties [49]. However, when a certain mechanical stiffness is needed, Irg provides a better stiffness without damaging the cells too much in comparison with VA-086®, where cell viability is affected greatly to obtain similar mechanical strength [50]. Scaffolds with VA-086® must be crosslinked twice as long as those with Irgacure to obtain a similar stiffness. Unfortunately, there is no working protocol to bioprint encapsulated spheroids with VA-086®. 15 min of UV crosslinking was needed to achieve stable constructs at 37 °C with a mean viability of 79% 7 days post-printing. The key limitation in photocrosslinking techniques for creating tissues is that exposure to harmful UV-light is needed and that photoinitiators may be cytotoxic in their precursor or radical form [51]. To avoid the use of UV-light, photoinitiators can be activated with blue (visible) light at 405 nm. This is obviously not as damaging to cell viability, but a co-initiator and co-monomer are needed to produce enough radicals. This is why we still prefer the use of the more toxic UV-induced photoinitiators. UV is also known to have limited penetration depth which might affect the overall polymerization efficiency for large constructs. Lin et al. [52] evaluated the effect of UV exposure on endothelial colony-forming cells and mesenchymal stem cells. They found that moderate UV light in UV spectrum of 320–500 nm at an intensity of 7.5 W cm^{-2} had >90% viability if exposed up to 200 s. We believe that the high number of cells in our constructs and the fact that spheroids are strong aggregations of differentiated cells, neither presence of Irg nor the UV-irradiation has a direct negative influence on the short-term viability of encapsulated spheroids. Photo-polymerization can be incorporated during the printing process: after each deposition of a layer, the construct is irradiated, which potentially shortens total exposure time since only a small layer of unexposed material needs to be penetrated by UV-light. No significant difference was found in viability between spheroids encapsulated in GelMA (80% ± 0.086) and spheroids encapsulated in GelMA and subsequently bioprinted (79% ± 0.078) after 7 days of culture ($p > 0.05$ and $n = 30$). This means that the extruding pressures of 0.050 MPa do not exhibit a negative influence on cell viability. Although gelatin provides a cell supportive environment to bioinks, its properties to protect cells from stress from bioprinting are low. This could mean that the physical structure of a spheroid offers slight protection against harmful factors of the bioprinting process. A decrease of 20% in viability in both the spheroids encapsulated in GelMA and bioprinted spheroids can be administered to the detrimental effects of crosslinking radicals and UV radiation. Zhao et al. [53] optimized nozzle temperature during bioprinting to improve cell viability. The authors reported 90% survival of HeLa cells at 25 °C nozzle temperature whereas 50% survival has been reported at 10 °C. This is in accordance to our nozzle temperature and room temperature of 23 °C. At 23 °C the applied pressure is around 0.050 MPa.

Building stable, large-volume AT by conventional tissue-engineering methods presents numerous challenges. Standard subcutaneous AT consists of differentiated adipocytes that make up only 90% of the total volume [54]. The main challenge is the establishment of a vascular system throughout the entire engineered tissue for long term survival in vivo. In mature AT, a well-defined vascular system is present with every adipocyte surrounded by one or more capillaries: AT triggers blood vessel formation and ECs promote preadipocyte differentiation [55]. A vascular system is a necessary component for AT engineering (long-term functionality) but also notoriously difficult to incorporate. Organ-on-chip technology is the closest we have come to achieve a functional unit but their integration into functional bioprinted constructs need more efforts to succeed [56]. In a next step, HUVEC's could be introduced in the 3D spheroids. Unfortunately, adipocytes and endothelial cells have disparate preferred culture conditions, requiring compromised solutions. Occhetta et al. [32] obtained good results co-culturing BM-MSCs with HUVEC. They note that BM-MSCs nor HUVECs cultured alone could form a surrounding ECM at comparable levels as the co-cultured constructs. Spheroid organization in vitro prior to implantation has been shown to improve in vivo angiogenesis [57].

We measured diameters of 153 ± 9.18 µm on day 1 and 101 ± 5.70 µm on day 13 of culture in ADM with a significant difference ($p < 0.001$) compared to spheroids cultured in SCM. Viability tends to be higher in ADM

compared to control medium in our experiments. The cells cultured in SCM expressed a pseudo-sphere shape due to the form of the microchip. After manipulation of ASC spheroids in SCM, a high tendency to disintegrate into single cells was observed and thus they could not be used as control for encapsulated spheroids. Our spheroids cultured in ADM showed compaction over time. The decrease of diameter and darker color of spheroids in our experiments may be explained by the increased cell-cell contact from neighboring cells in three-dimensional culture. We limited our research to 200 µm spheroids since the diffusion limit of oxygen is usually around 200 µm in vivo [58]. ASC spheroids release more hypoxia-related factors such as VEGF than ASCs grown in 2D culture [59]. Hypoxia could be beneficial for primitive cells but detrimental to differentiating cells such as ASC spheroids. Addition of angiogenic growth factors and endothelial precursor cells may address these issues, as investigated by De Moor et al. [39]. Generating blood vessels in artificial tissue deals with the ability of ECs to organize into blood vessels autonomously [60]. For in vitro TE, a rudimental interconnected tubular system must be available instantly, which matures into a genuine vascular structure for the fast integration of the engineered tissue to the host tissue. It is expected that this pre-structuring may guide the direction of growth into an interconnected capillary system. Recently, complex 3D tissue constructs containing parenchymal cells and vascular cells have been implanted in experimental models [61]. These studies show that functional tissue organoids can be constructed in vitro and implanted in tissue, with evidence of vascular integration between implanted and recipient circulations and restoration of tissue function by the organoids.

5 Conclusion

Bioprinting AT results from the combination of an increased need for breast reconstructions in today's society characterized by simplicity along with a low complication profile. Bioprinting ASC spheroids could revolutionize soft tissue reconstruction and counteract donor site morbidity, lengthy operations and microsurgical expertise. We provide a method to form nearly perfect round spheroids with minimal variability to be bioprinted in a desired 3D configuration. The ability to culture spheroids post-printing for extended periods of time, up to 14 days with excellent viability, has been achieved. Further research is needed to integrate endothelial precursor cells in spheroids to fabricate prevascularized constructs in vitro before implantation and to stimulate adipogenesis. This proof-of-concept enables researchers to further investigate such possibilities.

References

1. 2017. http://globocan.iarc.fr/Pages/fact_sheets_cancer.aspx.
2. Alaofi RK, Nassif MO, Al-Hajeili MR. Prophylactic mastectomy for the prevention of breast cancer: Review of the literature. Avicenna J Med. 2018;8:67–77.
3. Fracon S, et al. Patient satisfaction after breast reconstruction: implants vs. autologous tissues. Acta Chir Plast. 2018;59:120–8.
4. Blondeel PN. One hundred free DIEP flap breast reconstructions: a personal experience. Br J Plast Surg. 1999;52:104–11.
5. Critchley AC, et al. Current controversies in breast cancer surgery. Clin Oncol (R Coll Radiol). 2013;25:101–8.
6. N OH, et al. Hydrogels in adipose tissue engineering - potential application in post-mastectomy breast regeneration. J Tissue Eng Regen Med. 2018;12:2234–47.
7. Zhang YS, et al. 3D bioprinting for tissue and organ fabrication. Ann Biomed Eng. 2016;45:148–63.
8. Guiro K, Arinzeh TL. Bioengineering models for breast cancer research. Breast Cancer. 2015;9:57–70.
9. Laschke MW, Menger MD. Life is 3D: boosting spheroid function for tissue engineering. Trends Biotechnol. 2017;35:133–44.
10. Jakab K, et al. Tissue engineering by self-assembly of cells printed into topologically defined structures. Tissue Eng Part A. 2008;14:413–21.
11. Steinberg MS. Differential adhesion in morphogenesis: a modern view. Curr Opin Genet Dev. 2007;17:281–6.
12. Nichol JW, Khademhosseini A. Modular tissue engineering: engineering biological tissues from the bottom up. Soft Matter. 2009;5:1312–9.
13. Dean DM, et al. Rods, tori, and honeycombs: the directed self-assembly of microtissues with prescribed microscale geometries. FASEB J. 2007;21:4005–12.
14. Jakab K, et al. Tissue engineering by self-assembly and bioprinting of living cells. Biofabrication. 2010;2:022001.
15. Jakab K, et al. Relating cell and tissue mechanics: implications and applications. Dev Dyn. 2008;237:2438–49.
16. Miyagawa Y, et al. A microfabricated scaffold induces the spheroid formation of human bone marrow-derived mesenchymal progenitor cells and promotes efficient adipogenic differentiation. Tissue Eng Part A. 2011;17:513–21.
17. Turner PA, et al. Adipogenic differentiation of human adipose-derived stem cells grown as spheroids. Process Biochem. 2017;59:312–20.
18. Cheng NC, Wang S, Young TH. The influence of spheroid formation of human adipose-derived stem cells on chitosan films on stemness and differentiation capabilities. Biomaterials. 2012;33:1748–58.
19. Kapur SK, et al. Human adipose stem cells maintain proliferative, synthetic and multipotential properties when suspension cultured as self-assembling spheroids. Biofabrication. 2012;4:025004.
20. Murphy SV, Atala A. 3D bioprinting of tissues and organs. Nat Biotechnol. 2014;32:773–85.
21. Wang X, Liu C. 3D bioprinting of adipose-derived stem cells for organ manufacturing. Adv Exp Med Biol. 2018;1078:3–14.
22. Chang CC, et al. Direct-write bioprinting three-dimensional biohybrid systems for future regenerative therapies. J Biomed Mater Res B Appl Biomater. 2011;98:160–70.
23. Kang HW, et al. A 3D bioprinting system to produce human-scale tissue constructs with structural integrity. Nat Biotechnol. 2016;34:312–9.
24. Kolesky DB, et al. 3D bioprinting of vascularized, heterogeneous cell-laden tissue constructs. Adv Mater. 2014;26:3124–30.
25. Panwar A, LP Tan. Current status of bioinks for micro-extrusion-based 3D bioprinting. Molecules. 2016;21.

26. Vashi AV, et al. Adipose tissue engineering based on the controlled release of fibroblast growth factor-2 in a collagen matrix. Tissue Eng. 2006;12:3035–43.
27. Yao R, et al. Injectable cell/hydrogel microspheres induce the formation of fat lobule-like microtissues and vascularized adipose tissue regeneration. Biofabrication. 2012;4:045003.
28. Van Vlierberghe S, Dubruel P, Schacht E. Biopolymer-based hydrogels as scaffolds for tissue engineering applications: a review. Biomacromolecules. 2011;12:1387–408.
29. Tan H, et al. Injectable in situ forming biodegradable chitosan-hyaluronic acid based hydrogels for cartilage tissue engineering. Biomaterials. 2009;30:2499–506.
30. Wang Z, et al. A simple and high-resolution stereolithography-based 3D bioprinting system using visible light crosslinkable bioinks. Biofabrication. 2015;7:045009.
31. Billiet T, et al. The 3D printing of gelatin methacrylamide cell-laden tissue-engineered constructs with high cell viability. Biomaterials. 2014;35:49–62.
32. Occhetta P, et al. VA-086 methacrylate gelatine photopolymerizable hydrogels: a parametric study for highly biocompatible 3D cell embedding. J Biomed Mater Res A. 2015;103:2109–17.
33. Clevenger TN, et al. Cell-mediated remodeling of biomimetic encapsulating hydrogels triggered by adipogenic differentiation of adipose stem cells. J Tissue Eng. 2016;7:2041731416670482.
34. Huber B, et al. Methacrylated gelatin and mature adipocytes are promising components for adipose tissue engineering. J Biomater Appl. 2016;30:699–710.
35. Declercq HA, et al. Bone grafts engineered from human adipose-derived stem cells in dynamic 3D-environments. Biomaterials. 2013;34:1004–17.
36. Declercq H, et al. Isolation, proliferation and differentiation of osteoblastic cells to study cell/biomaterial interactions: comparison of different isolation techniques and source. Biomaterials. 2004;25:757–68.
37. Gevaert E, et al. High throughput micro-well generation of hepatocyte micro-aggregates for tissue engineering. PLoS ONE. 2014;9:e105171.
38. Berneel E, et al. Redifferentiation of high-throughput generated fibrochondrocyte micro-aggregates: impact of low oxygen tension. Cells Tissues Organs. 2016;202:369–81.
39. De Moor L, et al. High-throughput fabrication of vascularized spheroids for bioprinting. Biofabrication. 2018;10:035009.
40. Declercq HA, et al. Calcification as an indicator of osteoinductive capacity of biomaterials in osteoblastic cell cultures. Biomaterials. 2005;26:4964–74.
41. Rosen ED, et al. Transcriptional regulation of adipogenesis. Genes Dev. 2000;14:1293–307.
42. Fasshauer M, et al. Serum levels of the adipokine adipocyte fatty acid-binding protein are increased in preeclampsia. Am J Hypertens. 2008;21:582–6.
43. Mironov V, et al. Organ printing: tissue spheroids as building blocks. Biomaterials. 2009;30:2164–74.
44. Hurtley S. Spatial cell biology. Location, location, location. Introduction. Science. 2009;326:1205.
45. Kim SJ, et al. Hydrogels with an embossed surface: an all-in-one platform for mass production and culture of human adipose-derived stem cell spheroids. Biomaterials. 2018;188:198–212.
46. Pati F, et al. Biomimetic 3D tissue printing for soft tissue regeneration. Biomaterials. 2015;62:164–75.
47. Kayabolen A, et al. Native extracellular matrix/fibroin hydrogels for adipose tissue engineering with enhanced vascularization. Biomed Mater. 2017;12:035007.
48. Gungor-Ozkerim PS, et al. Bioinks for 3D bioprinting: an overview. Biomater Sci. 2018;6:915–46.
49. Wang Z, et al. An ultrafast hydrogel photocrosslinking method for direct laser bioprinting. RSC Adv. 2016;6:21099–104.
50. Zhu J, Marchant RE. Design properties of hydrogel tissue-engineering scaffolds. Expert Rev Med Devices. 2011;8:607–26.
51. Rouillard AD, et al. Methods for photocrosslinking alginate hydrogel scaffolds with high cell viability. Tissue Eng Part C Methods. 2011;17:173–9.
52. Lin RZ, et al. Transdermal regulation of vascular network bioengineering using a photopolymerizable methacrylated gelatin hydrogel. Biomaterials. 2013;34:6785–96.
53. Zhao Y, et al. Three-dimensional printing of Hela cells for cervical tumor model in vitro. Biofabrication. 2014;6:035001.
54. Eto H, et al. Characterization of structure and cellular components of aspirated and excised adipose tissue. Plast Reconstr Surg. 2009;124:1087–97.
55. Chhaya MP, et al. Sustained regeneration of high-volume adipose tissue for breast reconstruction using computer aided design and biomanufacturing. Biomaterials. 2015;52:551–60.
56. Moldovan NI, Hibino N, Nakayama K. Principles of the Kenzan method for robotic cell spheroid-based three-dimensional bioprinting. Tissue Eng Part B Rev. 2017;23:237–44.
57. Kim JH, et al. Therapeutic angiogenesis of three-dimensionally cultured adipose-derived stem cells in rat infarcted hearts. Cytotherapy. 2013;15:542–56.
58. Jain RK, et al. Engineering vascularized tissue. Nat Biotechnol. 2005;23:821–3.
59. Liu J, et al. Monitoring nutrient transport in tissue-engineered grafts. J Tissue Eng Regen Med. 2015;9:952–60.
60. Hoch E, Tovar GE, Borchers K. Bioprinting of artificial blood vessels: current approaches towards a demanding goal. Eur J Cardiothorac Surg. 2014;46:767–78.
61. Nunes SS, et al. Generation of a functional liver tissue mimic using adipose stromal vascular fraction cell-derived vasculatures. Sci Rep. 2013;3:2141.

Journal : **10856**
Article : **6374**

Springer
the language of science

Author Query Form

Please ensure you fill out your response to the queries raised below and return this form along with your corrections

Dear Author

During the process of typesetting your article, the following queries have arisen. Please check your typeset proof carefully against the queries listed below and mark the necessary changes either directly on the proof/online grid or in the 'Author's response' area provided below

Queries	Details Required	Author's Response
AQ1	Please check whether the designated corresponding author "Julien Colle" is correct.	
AQ2	Please check your article carefully, coordinate with any co-authors and enter all final edits clearly in the eproof, remembering to save frequently. Once corrections are submitted, we cannot routinely make further changes to the article.	
AQ3	Figure 8 was not cited in text. Please confirm the citation as provided now is okay.	
AQ4	Per style please provide "Conflict of interest" statement.	
AQ5	Please provide complete details for reference 1.	
AQ6	Please provide Page range in the reference 25.	